Rigid unit modes in sp-sp^2 hybridized carbon systems: Origin of negative thermal expansion

Cheol-Woon Kim, Seoung-Hun Kang, and Young-Kyun Kwon*

Department of Physics and Research Institute for Basic Sciences, Kyung Hee University, Seoul, 02447, Korea

(Received 21 July 2015; revised manuscript received 26 October 2015; published 22 December 2015)

Using density functional theory combined with quasiharmonic approximation, we investigate the thermal expansion behaviors of three different types (α, β, and γ) of graphyne, which is a two-dimensional carbon allotrope composed of sp and sp^2 bonds. For each type of graphyne, we obtain the temperature dependent area variation by minimizing its free energy calculated by considering all the phonon modes in the whole Brillouin zone. We find that all three types of graphyne exhibit negative in-plane thermal expansion up to $T \lesssim 1000$ K. The observed in-plane thermal contraction can be attributed partially to the ripple effect, similarly in graphene. The ripple effect itself, however, is not sufficient to explain the anomalously larger thermal contraction found in graphyne than in graphene. Our deliberate analysis on the phonon modes observed in graphyne enables us to reveal another source causing such thermal expansion anomaly. We find that there are particular phonon modes with frequencies of around a few hundreds of cm^{-1} existing exclusively in graphyne that may fill empty spaces resulting in area reduction. These modes are identified as "rigid unit modes" corresponding to the libration of each rigid unit composed of sp^2 bonds.

DOI: 10.1103/PhysRevB.92.245434 PACS number(s): 62.23.Kn, 81.05.Zx, 81.07.De, 61.46.−w

I. INTRODUCTION

Various carbon allotropes based on sp^2 hybridization, such as fullerenes [1], nanotubes [2], and graphene [3], have been intensively studied during the last few decades, since their first discoveries. Their unique properties are basically related to the hexagonal geometry and the Dirac cones in the electronic structure of graphene [4–6], which is a base material to form other sp^2-bonded carbon allotropes. To make use of graphene in future nanoelectronics, however, it is indispensable to open an energy gap at the Fermi level E_F. Although lots of attempts have been made to open a band gap [7–14], nothing has yet come along for practical applications. As a separate approach, sundry efforts have been made to search for other two-dimensional (2D) allotropes intrinsically possessing an energy gap at E_F to be used as graphene substitutes in electronic applications [15].

A new 2D layered carbon allotrope called graphyne was proposed in 1987 [16]. It can be geometrically generated from graphene by inserting a single acetylenic linkage (AL) consisting of two sp-hybridized carbon atoms into a bond in graphene composed of sp^2-hybridized carbon atoms only. Since there are a number of ways of inserting ALs, many different types of graphyne can be formed. Among them were mainly considered three types with a hexagonal symmetry, which are classified by the number of sp-bonded or doubly coordinated atoms, N_{sp}, which is equivalent to the number of ALs attached to each sp^2-hybridized or triply coordinated carbon atom: α-, β-, and γ-graphyne. As shown in Figs. 1(a)–1(c), three, two, or one AL(s) are connected to every sp^2-hybridized carbon atom in α-, β-, or γ-graphyne, respectively.

Theoretical studies showed that both α- and β-graphyne structures possess the Dirac cones near E_F in its Brillouin zone (BZ) representing their semimetallic characteristics like in graphene [17–23]. Interestingly, on the other hand, γ-graphyne, known for the most stable graphyne by far, is an intrinsic semiconductor with a direct band gap of 0.46 eV at M points [17,20,24]. The existence of the band gap was ascribed by the Peierls instability resulting in the wave function localization at the triple bonds [20]. It is, therefore, expected that γ-graphyne could be made use of as a semiconducting component in future nanoelectronics.

Although graphyne has not yet been realized in a crystalline form, various research groups have endeavored to synthesize it. As a result, it was reported that graphyne subunits resembling γ-graphyne were successfully synthesized [25–27]. Moreover, one of their cousin structures with two sequentially connected ALs, instead of a single AL as in γ-graphyne, called graphdiyne, was also discovered in the form of sheet [28], as well as in a tubular form [29]. Since our calculation revealed that β-graphyne and γ-graphyne are even more stable than graphdiyne, as shown in Fig. 1(d), which was also verified by other studies [24,30,31], we expect that they will be definitely synthesized in the near future. Compared to the structural and electronic properties of α-, β-, and γ-graphyne that have been intensively studied as discussed above, there have not been many studies on their thermal and thermal expansion (TE) behaviors [22,23,32], which are also necessary properties to be disclosed in advance for them to be utilized as various devices in future nanoelectronics.

It is well known that most materials expand thermally with a very different material-dependent linear TE coefficient (TEC) of 10^{-7}–10^{-4} mainly due to the atomic vibration under asymmetric potential. In almost all devices and equipment, such a TE usually becomes a critical problem deteriorating their performance and lifetime. There have been, on the other hand, several reports revealing materials with a negative TEC (NTEC), such as graphite [33], carbon nanotubes [34,35], zirconium tungstate (ZrW_2O_8) [36], perovskite oxides [37–39], and Invar alloys [40,41]. The NTE behaviors in these materials are attributed to a ripple effect, bending/twisting modes, rigid unit modes (RUMs) [42,43], atomic radius contraction [44], or magnetovolume effects [45]. Researchers have made various attempts to make composites containing NTE materials, such as ZrW_2O_8 [46–48] and β-eucryptite [49], as a TE

*Corresponding author: ykkwon@khu.ac.kr

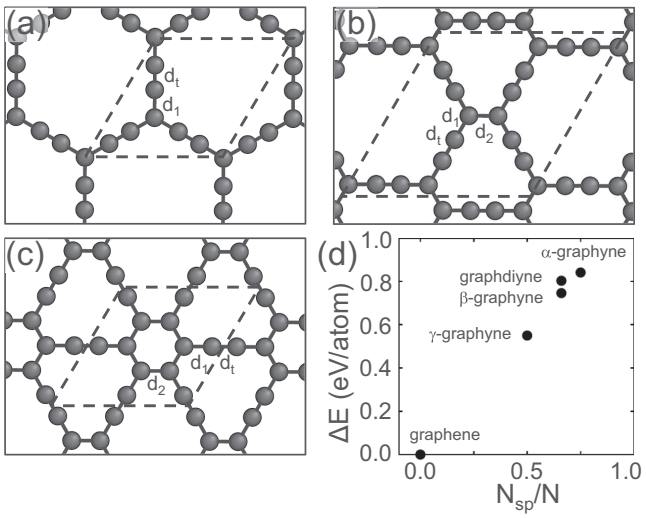

FIG. 1. Equilibrium structures of (a) α-graphyne, (b) β-graphyne, and (c) γ-graphyne. Respective hexagonal unit cells are depicted by dashed parallelograms. Nonequivalent bonds in each type of graphyne are denoted by d_1, d_2, and d_t. d_1 and d_2, which are single-bond like, represent a bond between an sp^2-bonded (or triply coordinated) and an sp-bonded (or doubly coordinated) atoms, and one between two triply coordinated atoms, respectively, whereas d_t designates a triple bond between two sp atoms in every acetylenic linkage. (d) Cohesive energy comparison of three types of graphyne and graphdiyne with respect to graphene as a function of N_{sp}/N, where N_{sp} and N are the number of sp-bonded or doubly coordinated atoms and the total number of atoms in the unit cell, respectively.

compensator, expecting them to be high-performance composites with near zero TE. It was indeed shown that TE can be suppressed in molten aluminum alloy with NTE manganese antiperovskites [50].

In this paper, we report our investigation on the NTE observed in sp–sp^2 hybridized carbon systems. Such a TE anomaly is caused not only by the ripple effect due to the flexural modes as observed in graphene, but also by the RUMs, which have not yet been identified in two-dimensional graphitic carbon systems, but observed in 2D perovskites [51]. The thermal properties and TE behaviors of α-, β-, and γ-graphyne were investigated by first-principles calculations of temperature- and volume-dependent free energies from the phonon properties. Similar to graphene, all three configurations contract with temperature up to $T \approx 1000$ K, but the absolute values of their TECs are much larger than that of graphene especially at low temperatures. Based on our thorough investigation on their phonon modes, we attributed such thermal contraction behaviors not only to the ripple effect as in graphene, but also to RUMs corresponding to libration motions of rigid units composed of sp^2 bonds only.

II. COMPUTATIONAL DETAILS

To investigate the TE behaviors of three types of graphyne, we first obtained their equilibrium structures by carrying out first-principles calculations within the density functional theory [52], as implemented in the Vienna *ab initio* simulation package (VASP) [53,54], while adjusting three different carbon-carbon bonds, and thus the lattice constant of each graphyne as discussed in Sec. III. Projector augmented wave potentials [55,56] was employed to describe the valence electrons, and the electronic wave functions were expanded by a plane wave basis set with the cutoff energy of 450 eV. The exchange-correlation functional was treated with the Perdew-Burke-Ernzerhof parametrization [57] of the generalized gradient approximation. To mimic single-layered graphyne, we introduced a vacuum region with 15 Å along the c axis perpendicular to the sheet. The BZ was sampled using a Γ-centered $10\times10\times1$ k grid for the primitive unit cell of each type of graphyne. Although the primitive cell size of β-graphyne is larger than the other types, the same k grid was employed for precise calculation for β-graphyne because there were earlier studies on β-graphyne showing inconsistent results on structural stability [22,23].

The phonon dispersion relations were computed by applying the finite displacement (FD) method [58,59] for $3\times3\times1$ supercells. The corresponding reduced BZs were sampled by $3\times3\times1$ k-point meshes. In each supercell, we solved the secular equation of dynamical matrix constructed at every wave vector $\mathbf{q}$ from the force constant matrices computed under FD to obtain the phonon dispersion relation. To investigate thermal properties, we employed quasiharmonic approximation (QHA) [60,61], in which the Helmholtz free energy of a 2D graphyne sheet was calculated by

$$F(T,A) = U(A) + \frac{1}{2}\sum_{\mathbf{q},n}\hbar\omega_{\mathbf{q},n} + k_BT\sum_{\mathbf{q},n}\ln\left\{1-\exp\left(-\frac{\hbar\omega_{\mathbf{q},n}}{k_BT}\right)\right\}, \quad (1)$$

where $\hbar$ and k_B are the reduced Planck constant, and the Boltzmann constant, respectively; and $\omega_{\mathbf{q},n}$ is the phonon frequency with the wave vectors $\mathbf{q}$ and the mode indices n. In Eq. (1), the first term $U(A)$ is the system internal energy with a constant area A at $T = 0$; the second term represents the vibrational zero-point energy of the lattice; and the last term corresponds to the phonon contribution to the free energy in QHA [60,61]. $U(A)$ and $\omega_{\mathbf{q},n}$ were evaluated at 12 different area points. $F(T,A)$ was fitted to the integral form of the Vinet equation of state [62] to obtain the minimum values of the thermodynamic functions with respect to the area, and thus the equilibrium area, $A(T)$, as a function of temperature. TE behaviors of three types of graphyne sheets were explored by calculating the area TEC $\alpha_S(T)$ as a function of T,

$$\alpha_S(T) = \frac{1}{A(T)}\frac{dA(T)}{dT}. \quad (2)$$

III. RESULTS AND DISCUSSION

We first searched for the equilibrium structures of three kinds of graphyne, which are indispensable to their phonon dispersion relations and thermal properties. Graphyne can be made by replacing all or some bonds in graphene by an AL (—C ≡ C—). Among numerous different types of graphyne produced in this way, we only focused on three types of graphyne, α, β, and γ, which are highly symmetric in a hexagonal lattice relative to the other types. The α-graphyne

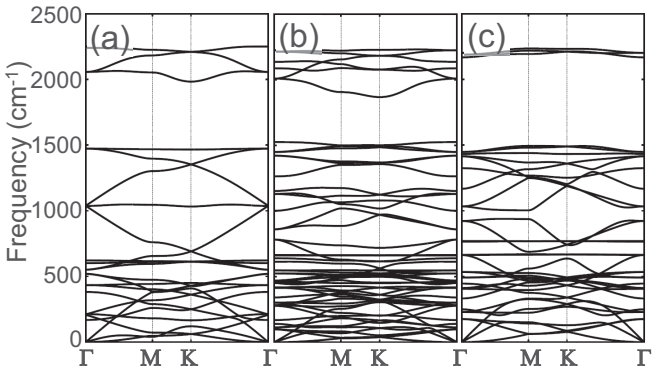

FIG. 2. The phonon dispersion relations of (a) α-graphyne, (b) β-graphyne, and (c) γ-graphyne along the high symmetry lines in 2D hexagonal Brillouin zones.

can be made by a complete substitution for graphitic bonds, while the β-graphyne and γ-graphyne can be formed by two-thirds and one-third substitutions, respectively. In these types of graphyne, there are at most three nonequivalent carbon-carbon bonds, d_1, d_2, and d_t. Single-bond-like d_1 and d_2 represent bonds from a sp^2 atom to a neighboring sp and sp^2 atom, respectively, while a triple-bond d_t describes a bond between two neighboring sp atoms forming an AL together with two d_1 bonds.

For each graphyne, we completely scanned the whole energy surface while adjusting the bond length of three nonequivalent carbon-carbon bonds, d_1, d_2, and d_t, keeping its hexagonal symmetry. Note that there are no d_2 bonds in α-graphyne, and the lattice constant of each unit cell is uniquely determined for each set of given d_1, d_2, and d_t. The equilibrium structures of three types of graphyne were determined at the minimum energy point in each energy surface, and shown in Figs. 1(a)–1(c), where their hexagonal lattices were depicted by dashed parallelograms representing their unit cells. Two nonequivalent bonds in the α-graphyne were calculated to be $d_1 = 1.397$ Å and $d_t = 1.230$ Å with lattice constant of $a_{\rm eq} = 6.969$ Å. For the β-graphyne (γ-graphyne), on the other hand, its calculated lattice constant and three nonequivalent bond lengths are $a_{\rm eq} = 9.480$ Å (6.890 Å), $d_1 = 1.389$ Å (1.408 Å), $d_2 = 1.458$ Å (1.426 Å), and $d_t = 1.232$ Å (1.223 Å). Our determined structural parameters are in good agreement with other studies [20,23].

To compare the structural stability of three types of graphyne, we evaluated their cohesive energies with respect to that of graphene as a function of N_{sp}/N, where N_{sp} and N are the number of sp-bonded or doubly coordinated atoms, and N and the total number of atoms in the unit cell, respectively. As displayed in Fig. 1(d), these types of graphyne are only 0.6–0.8 eV/atom less stable than graphene. This tendency agrees well with quantum Monte Carlo calculations [24,30,31]. Especially, the γ-graphyne and β-graphyne are even more stable than graphdiyne, which was already reported to be synthesized [28,29], expecting to be synthesized as well.

Using $3 \times 3 \times 1$-repeated supercells of the equilibrium structures, we calculated the phonon dispersion relations of all three types of graphyne as shown in Fig. 2, and identified all the phonon branches by analyzing their corresponding eigenvectors. We found in all cases that there are three acoustic phonon branches below $\nu \approx 400\,{\rm cm}^{-1}$, two in-plane modes with a linear dispersion and one quadratic out-of-plane mode near Γ point. We did not find any imaginary frequencies in all the types of graphyne indicating their structural stability. Our phonon results are in good agreement with other studies [22,23], except that there were a few different features in previous studies such as Kohn anomalies [22] and imaginary phonon frequencies [23], especially for β-graphyne. The Kohn anomalies were observed by considering electron-phonon matrix elements [22], which we did not consider explicitly. The imaginary phonon frequencies were, on the other hand, due to Γ point only calculation with a small supercell [23].

Compared to graphene with its maximum frequency of $\lesssim 1600\,{\rm cm}^{-1}$ [63], graphyne exhibits even higher phonon branches dispersed at $\nu \gtrsim 2000\,{\rm cm}^{-1}$. These high frequency modes correspond mainly to the stretching vibration of the triple bonds d_t with larger force constants than single-bond-like d_1 and d_2, which generate graphene-like phonon modes at $\nu \lesssim 1500\,{\rm cm}^{-1}$ below a large frequency gap of $\Delta\nu \approx 500\,{\rm cm}^{-1}$, as displayed in Fig. 2. The existence of such a large frequency gap implies that the vibration of d_t bond stretching modes is strongly protected from being scattered by the graphene-like modes by the energy conservation law [64]. Another phonon gap of $\Delta\nu \approx 32$, 78, or 67 cm^{-1}, was also observed near $\nu \approx 500$, 750, or 1000 cm^{-1} for α-, β-, or γ-graphyne, respectively. We found that the d_1 and d_2 stretching modes are dispersed above the gap, while all the bending modes including optical flexural modes are settled below. Note there is an exception in the α-graphyne as displayed in Fig. 2(a) that there are two flat modes identified as optical flexural modes located at $\nu \approx 602$ and 622 cm^{-1} above the gap. Therefore, in the α-graphyne, these optical flexural phonons can be scattered by the stretching phonons, while in the other types of graphyne, they are located at similar frequencies, but below their frequency gap, as shown in Figs. 2(b) and 2(c), which protects them from being scattered by their corresponding d_1 and d_2 stretching modes.

To evaluate the Helmholtz free energy, we used Eq. (1) with the phonon dispersion relations $\omega_{\mathbf{q},n}$ calculated at 12 different area points, based on QHA. For each type of graphyne, the calculated Helmholtz free energy was plotted as a function of temperature and area in a color-coded map as displayed in Fig. 3. Note that color-coded energy values clearly represent that the γ-graphyne is more stable than the other two types. The temperature dependence of the equilibrium area $A(T)$ was obtained by minimizing the thermodynamic functions with respect to the area as denoted with the black solid line on each color-coded map in Fig. 3.

We explored the TE behaviors of three types of graphyne as well as graphene for comparison by evaluating the temperature dependence of change in each system's area with respect to the zero-temperature area, $\Delta A/A_0 \equiv [A(T) - A_0]/A_0$, and its area TEC $\alpha_s(T)$ given by Eq. (2). It was found that similar to graphene, all three types of graphyne contract as temperature increases up to $T \approx 1000$ K, as shown in Fig. 4(a). Such an area shrink observed in a 2D sheet was attributed to its flexural modes, which are mainly responsible for the ripple effect [65], as in graphene [32,63], and in graphyne [23,32]. We confirmed the contribution of flexural modes of graphyne

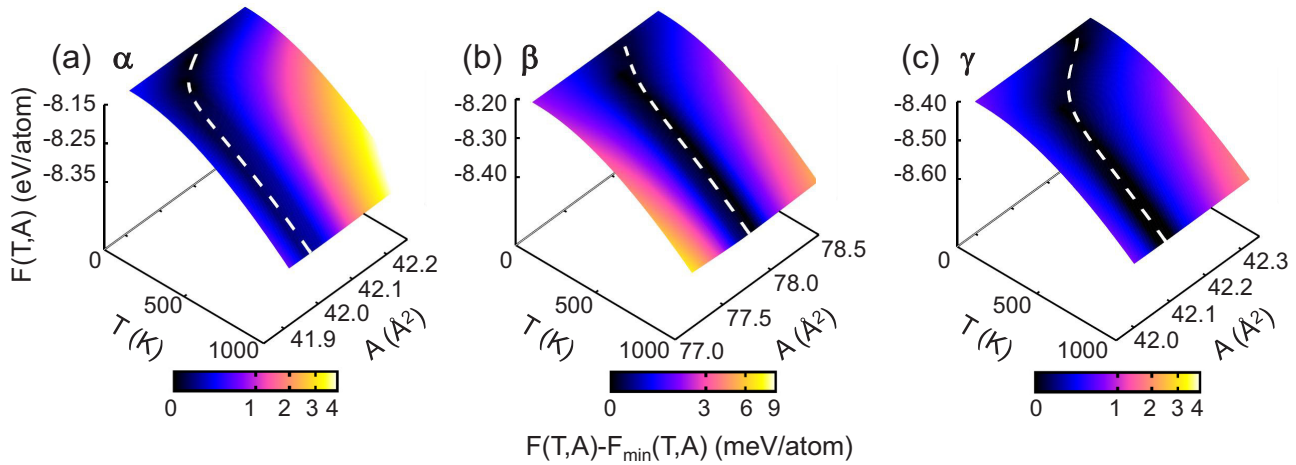

FIG. 3. (Color online) Helmholtz free energy as a function of temperature and area calculated using Eq. (1) for (a) α-graphyne, (b) β-graphyne, and (c) γ-graphyne. The free energy values are represented by height along the $F(T,A)$ axis, whereas the relative values $\Delta F(T,A) \equiv F(T,A) - \min_A F(T,A)$ of the free energy with respect to the minimum value for a given temperature are depicted by color-coded maps. The white dashed line on each plot indicates the free energy minima yielding the equilibrium area at a given temperature. The relative free energy values are represented by a color scheme shown by the color bar below.

to NTE by evaluating their corresponding mode Grüneisen parameters, $\gamma_{\mathbf{q},n}$, defined as

$$\gamma_{\mathbf{q},n} = -\frac{\partial \log \omega_{\mathbf{q},n}}{\partial \log V} = -\frac{V}{\omega_{\mathbf{q},n}} \frac{\partial \omega_{\mathbf{q},n}}{\partial V}, \tag{3}$$

to be negative. These mode Grüneisen parameters are related to how the corresponding phonon modes change as the volume changes and combined to evaluate the macroscopic Grüneisen parameter γ as

$$\gamma = \frac{\sum_{\mathbf{q},n} \gamma_{\mathbf{q},n} c_{\mathbf{q},n}}{\sum_{\mathbf{q},n} c_{\mathbf{q},n}}, \tag{4}$$

where $c_{\mathbf{q},n}$ are the mode contributions to the heat capacity. It is known that γ is proportional to the TEC α, which means the negative γ yields the NTEC.

Using Eq. (2), we also calculated the TECs of three types of graphyne as well as graphene. Compared to our calculated TEC values of graphene, which are in good agreement with previous studies [32,63], it was observed that graphyne exhibits significantly lower TEC values than graphene especially at low temperatures as shown in Fig. 4(b), which cannot be fully understood only by the flexural modes responsible for the ripple effect. To scrutinize such large differences, we thoroughly inspected the real-space vibrations of all the phonon modes by visualizing their corresponding eigenvectors together with mode Grüneisen parameters at different wave vectors $\mathbf{q}$ and mode indices n, and found intriguing unexpected vibrational modes, which we classified as RUMs [42]. It has already been known that the RUMs and quasi RUMs involving a little distortion of rigid polyhedra are major causes of NTE occurred in an oxide framework consisting of rigid polyhedra, such as MO_4 and MO_6, where M and O are a metal cation and oxygen [66,67], although it was reported that there is no simple correlation between NTE and RUMs [68].

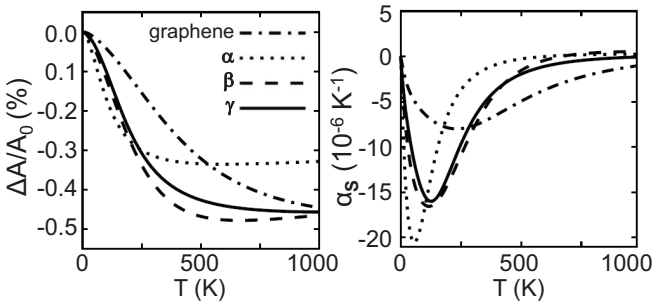

FIG. 4. (a) Temperature dependence of the ratio of area expansion to the reference area at $T = 0$ K, $\Delta A/A_0$ in the unit of percentage %, and (b) the corresponding area thermal expansion coefficient, $\alpha_S(T)$, defined by Eq. (2), in the unit of 10^{-6} K^{-1}, of α-graphyne (dotted line), β-graphyne (dashed line), and γ-graphyne (solid line) as well as of graphene (dash-dotted line) for comparison.

To verify the effect of RUMs on NTE of 2D graphyne, we considered only one RUM in each type of graphyne, while freezing out all the other modes. Figures 5(a)–5(c) show real-space visualization of typical RUMs (in the right) observed at $\nu \approx 382$, 277, and 249 cm^{-1} in α-, β-, and γ-graphyne, respectively, in tandem with their corresponding equilibrium configurations (in the left). Note that the structures representing the RUMs were exaggeratedly rotated to show them clearly. We also found that there are other RUMs contributing to NTE (see Fig. S1 in Supplemental Material [69]). The corresponding rigid units are denoted, respectively, by gray polygons of a triangle, a rectangle, and a hexagon, each of which encloses the sp^2 carbon atoms connected with d_1 and d_2 bonds.

During the libration mode of the rigid unit in each graphyne, every AL becomes bent and thus the d_t bonds are lengthened as shown in Figs. 5(a)–5(c). We found that such lengthened bonds can be compensated by filling an empty space or reducing the area size. To clarify the correlation between these RUMs and NTE in the graphyne systems and to analyze the size reduction quantitatively, we calculated the relative energy of

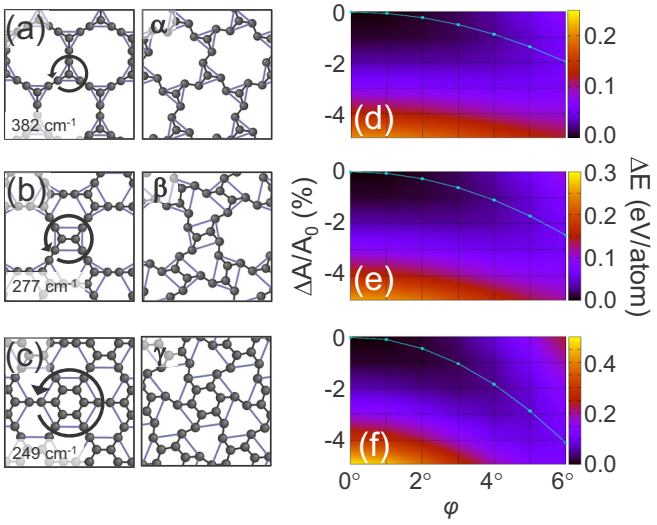

FIG. 5. (Color online) Real-space visualization of typical rigid unit modes observed in (a) α-graphyne, (b) β-graphyne, and (c) γ-graphyne, respectively, with $\nu \approx 382$, 277, and 249 cm^{-1}. Each local rigid unit is represented by a gray polygon [triangle, square, or hexagon in (a), (b), or (c), respectively] surrounding sp^2 carbon atoms with d_1 and d_2 bonds. Each equilibrium structure is depicted in the left box, while the right box shows a snapshot of rigid units rotated counterclockwise corresponding to the selected RUM. Relative energy map color coded as a function of $\Delta A/A_0$ and rotation angle φ of each rigid unit calculated for (d) α-graphyne, (e) β-graphyne, and (f) γ-graphyne. Cyan-colored solid line with dots indicates the area contraction determined by the minimum energy for given φ. Energy values are given in terms of the equilibrium energy of each graphyne.

each type of graphyne as a function of the area strain $\Delta A/A_0$, and the rotation angle φ of each rigid unit, while freezing out all the other modes. Figures 5(d)–5(f) display the color-coded energy map, in which the area reduction was estimated by searching for the minimum values of the relative energy ΔE for a given φ, as depicted by the cyan-colored line with dots. Since the maximum rotation angle may increase with temperature, RUMs as well as the ripple effects may contribute to the area reduction (see Table S1 in the Supplemental Material for the evaluated libration angle φ and the area reduction $\Delta A/A_0$ at $T = 600$ and 900 K). The mode Grüneisen parameters corresponding to the RUMs was also calculated to be negative as similarly in the flexural modes contributing to the ripple effects (see Fig. S2 in Supplemental Material).

IV. CONCLUSIONS

We presented the phonon dispersion relations and the thermal expansion behaviors of α-, β- and γ-graphyne using the density functional theory. Our calculated phonon dispersion relations showed that there were no imaginary frequencies implying their structural stability. Their high-frequency modes at $\nu \approx 2000\,\mathrm{cm}^{-1}$ correspond to the stretching modes of the triple bonds d_t, which are protected by the large frequency gap from being scattered by graphene-like modes of d_1 and d_2 bonds. Similarly, the stretching modes of d_1 and d_2 bonds can also be protected from being scattered by their bending modes, since the latter modes are separately located below another frequency gap, with an exception in α-graphyne. Our quasiharmonic approximation calculations revealed that all types of graphyne exhibit negative thermal expansion as in other 2D materials, but they have much larger values in negative thermal expansion coefficients than graphene. This significant discrepancy was resolved by identifying the rigid unit modes, which were first observed in 2D carbon graphitic structures. We found that not only the ripple effect originating from the flexural modes, but also the rigid unit modes are strongly responsible for the negative thermal expansion in graphyne.

ACKNOWLEDGMENTS

We thank Hyeonsu Lee for fruitful discussion. This work was supported by a grant (Grant No. KHU-20090508) from Kyung Hee University. Some portion of our computational work was done using the resources of the Korea Institute of Science and Technology Information (KISTI) Supercomputing Center (KSC-2014-C2-028 and KSC-2014-G2-001).

[1] H. W. Kroto, J. R. Heath, S. C. O'Brien, R. F. Curl, and R. E. Smalley, Nature (London) **318**, 162 (1985).
[2] S. Iijima, Nature(London) **354**, 56 (1991).
[3] K. S. Novoselov, A. K. Geim, S. V. Morozov, D. Jiang, Y. Zhang, S. V. Dubonos, I. V. Grigorieva, and A. A. Firsov, Science **306**, 666 (2004).
[4] Y. Zhang, Y.-W. Tan, H. L. Stormer, and P. Kim, Nature (London) **438**, 201 (2005).
[5] K. S. Novoselov, A. K. Geim, S. V. Morozov, D. Jiang, M. I. Katsnelson, I. V. Grigorieva, S. V. Dubonos, and A. A. Firsov, Nature(London) **438**, 197 (2005).
[6] A. H. Castro Neto, N. M. R. Peres, K. S. Novoselov, A. K. Geim, and F. Guinea, Rev. Mod. Phys. **81**, 109 (2009).
[7] H. Şahin and S. Ciraci, Phys. Rev. B **84**, 035452 (2011).
[8] S. Kim, J. Ihm, H. J. Choi, and Y.-W. Son, Phys. Rev. Lett. **100**, 176802 (2008).
[9] Y.-W. Son, M. L. Cohen, and S. G. Louie, Phys. Rev. Lett. **97**, 216803 (2006).
[10] S. Y. Zhou, G.-H. Gweon, A. V. Fedorov, P. N. First, W. A. de Heer, D.-H. Lee, F. Guinea, A. H. Castro Neto, and A. Lanzara, Nat. Mater. **6**, 770 (2007).
[11] D. Yu, E. M. Lupton, M. Liu, W. Liu, and F. Liu, Nano Res. **1**, 56 (2008).
[12] W. Liu, Z. F. Wang, Q. W. Shi, J. Yang, and F. Liu, Phys. Rev. B **80**, 233405 (2009).
[13] Y.-K. Kwon, J. Korean Phys. Soc. **57**, 778 (2010).
[14] J. Haskins, A. Kınacı, C. Sevik, H. Sevincli, G. Cuniberti, and T. Çağn, ACS Nano **5**, 3779 (2011).
[15] A. Hirsch, Nat. Mater. **9**, 868 (2010).
[16] R. H. Baughman, J. Chem. Phys. **87**, 6687 (1987).
[17] J. Kang, J. Li, F. Wu, S.-S. Li, and J.-B. Xia, J. Phys. Chem. C **115**, 20466 (2011).

[18] J. Zhou, K. Lv, Q. Wang, X. S. Chen, Q. Sun, and P. Jena, J. Chem. Phys. **134**, 174701 (2011).
[19] D. Malko, C. Neiss, F. Viñes, and A. Görling, Phys. Rev. Lett. **108**, 086804 (2012).
[20] B. G. Kim and H. J. Choi, Phys. Rev. B **86**, 115435 (2012).
[21] Z. Liu, G. Yu, H. Yao, L. Liu, L. Jiang, and Y. Zheng, New J. Phys. **14**, 113007 (2012).
[22] V. N. Popov and P. Lambin, Phys. Rev. B **88**, 075427 (2013).
[23] N. K. Perkgöz and C. Sevik, Nanotechnology **25**, 185701 (2014).
[24] A. L. Ivanovskii, Prog. Solid State Chem. **41**, 1 (2013).
[25] E. L. Spitler, C. A. J. Ii, and M. M. Haley, Chem. Rev. **106**, 5344 (2006).
[26] M. M. Haley, Pure Appl. Chem. **80**, 519 (2008).
[27] T. Takeda, A. G. Fix, and M. M. Haley, Org. Lett. **12**, 3824 (2010).
[28] G. Li, Y. Li, H. Liu, Y. Guo, Y. Li, and D. Zhu, Chem. Commun. (Cambridge, U. K.) **46**, 3256 (2010).
[29] X. Qian, Z. Ning, Y. Li, H. Liu, C. Ouyang, Q. Chen, and Y. Li, Dalton Trans. **41**, 730 (2012).
[30] W.-J. Yin, Y.-E. Xie, L.-M. Liu, R.-Z. Wang, X.-L. Wei, L. Lau, J.-X. Zhong, and Y.-P. Chen, J. Mater. Chem. A **1**, 5341 (2013).
[31] H. Shin, S. Kang, J. Koo, H. Lee, J. Kim, and Y. Kwon, J. Chem. Phys. **140**, 114702 (2014).
[32] T. Shao, B. Wen, R. Melnik, S. Yao, Y. Kawazoe, and Y. Tian, J. Chem. Phys. **137**, 194901 (2012).
[33] J. B. Nelson and D. P. Riley, Proc. Phys. Soc. **57**, 477 (1945).
[34] Y.-K. Kwon, S. Berber, and D. Tománek, Phys. Rev. Lett. **92**, 015901 (2004).
[35] Y.-K. Kwon, S. Berber, and D. Tománek, Phys. Rev. Lett. **94**, 209702 (2005).
[36] C. Martinek and F. A. Hummel, J. Am. Ceram. Soc. **51**, 227 (1968).
[37] Y. Long, N. Hayashi, T. Saito, M. Azuma, S. Muranaka, and Y. Shimakawa, Nature (London) **458**, 60 (2009).
[38] Y. Long and Y. Shimakawa, New J. Phys. **12**, 063029 (2010).
[39] M. Azuma, W.-t. Chen, H. Seki, M. Czapski, S. Olga, K. Oka, M. Mizumaki, T. Watanuki, N. Ishimatsu, N. Kawamura *et al.*, Nat. Commun. **2**, 347 (2011).
[40] T. Moriya and K. Usami, Solid State Commun. **88**, 911 (1993).
[41] K. Sumiyama, M. Shiga, M. Morioka, and Y. Nakamura, J. Phys. F **9**, 1665 (1979).
[42] K. D. Hammonds, M. T. Dove, A. P. Giddy, V. Heine, and B. Winkler, Am. Mineral. **81**, 1057 (1996).
[43] M. G. Tucker, A. L. Goodwin, M. T. Dove, D. A. Keen, S. A. Wells, and J. S. O. Evans, Phys. Rev. Lett. **95**, 255501 (2005).
[44] J. Arvanitidis, K. Papagelis, S. Margadonna, K. Prassides, and A. N. Fitch, Nature (London) **425**, 599 (2003).
[45] C. E. Guillaume, C. R. Acad. Sci. **125**, 235 (1897).
[46] L. M. Sullivan and C. M. Lukehart, Chem. Mater. **17**, 2136 (2005).
[47] C. Verdon, Scr. Mater. **36**, 1075 (1997).
[48] H. Holzer and D. C. Dunand, J. Mater. Res. **14**, 780 (2011).
[49] Z. W. Xue, L. D. Wang, Z. Liu, and W. D. Fei, Scr. Mater. **62**, 867 (2010).
[50] M. Ishii, H. Shimojima, H. Takagi, K. Takenaka, and M. Watanabe, Patent Application No. US 10/479,044 (2008).
[51] A. L. Goodwin and C. J. Kepert, Phys. Rev. B **71**, 140301 (2005).
[52] W. Kohn and L. J. Sham, Phys. Rev. **140**, A1133 (1965).
[53] G. Kresse and J. Furthmüller, Phys. Rev. B **54**, 11169 (1996).
[54] G. Kresse and J. Hafner, Phys. Rev. B **47**, 558 (1993).
[55] P. E. Blöchl, Phys. Rev. B **50**, 17953 (1994).
[56] G. Kresse and D. Joubert, Phys. Rev. B **59**, 1758 (1999).
[57] J. P. Perdew, K. Burke, and M. Ernzerhof, Phys. Rev. Lett. **77**, 3865 (1996).
[58] K. Parlinski, Z.-. Q. Li, and Y. Kawazoe, Phys. Rev. Lett. **78**, 4063 (1997).
[59] A. Togo, F. Oba, and I. Tanaka, Phys. Rev. B **78**, 134106 (2008).
[60] P. Pavone, K. Karch, O. Schütt, W. Windl, D. Strauch, P. Giannozzi, and S. Baroni, Phys. Rev. B **48**, 3156 (1993).
[61] A. Togo, L. Chaput, I. Tanaka, and G. Hug, Phys. Rev. B **81**, 174301 (2010).
[62] P. Vinet and J. H. Rose, J. Phys.: Condens. Matter **1**, 1941 (1989).
[63] N. Mounet and N. Marzari, Phys. Rev. B **71**, 205214 (2005).
[64] J.-W. Jiang, Nanoscale **6**, 8326 (2014).
[65] I. M. Lifshitz, Zh. Eksp. Teor. Fiz. **22**, 475 (1952).
[66] A. K. A. Pryde, K. D. Hammonds, M. T. Dove, V. Heine, J. D. Gale, and M. C. Warren, J. Phys.: Condens. Matter **8**, 10973 (1996).
[67] W. Miller, C. W. Smith, D. S. Mackenzie, and K. E. Evans, J. Mater. Sci. **44**, 5441 (2009).
[68] J. Z. Tao and A. W. Sleight, J. Solid State Chem. **173**, 442 (2003).
[69] See Supplemental Material at http://link.aps.org/supplemental/10.1103/PhysRevB.92.245434 for detailed description of rigid unit modes and flexural modes contributing to negative thermal expansion and their corresponding mode Gruneisen parameters.